Multimed Tools Appl (2017) 76:17719–17734
DOI 10.1007/s11042-015-2960-3

Change detection method for remote sensing images based on an improved Markov random field

Wei Gu[1] · **Zhihan Lv**[2] · **Ming Hao**[3]

Received: 20 July 2015 / Revised: 27 August 2015 / Accepted: 17 September 2015 /
Published online: 26 September 2015

Abstract The fixed weights between the center pixel and neighboring pixels are used in the traditional Markov random field for change detection, which will easily cause the overuse of spatial neighborhood information. Besides the traditional label field cannot accurately identify the spatial relations between neighborhood pixels. To solve these problems, this study proposes a change detection method based on an improved MRF. Linear weights are designed for dividing unchanged, uncertain and changed pixels of the difference image, and spatial attraction model is introduced to refine the spatial neighborhood relations, which aims to enhance the accuracy of spatial information in MRF. The experimental results indicate that the proposed method can effectively enhance the accuracy of change detection.

Keywords Markov random field · Fuzzy c-means · Linear weights · Spatial attraction model · Spatial information

1 Introduction

Change detection aims founding changes occurred on the Earth surface by analyzing remotely sensed images acquired in the same geographical area at two or more different times [5, 13]. Moreover, it is widely used to detect disasters, monitor environmental changes and identify land use/land cover.

Markov random field (MRF) is an image processing method that comprehensively utilizes spectral and spatial information [4]. With the adoption of maximum a posteriori (MAP)

✉ Wei Gu
guweimtap@163.com

[1] State Key Laboratory of Coal Resources and Mine Safety, School of Mines, China University of Mining & Technology, Xuzhou 221116, China

[2] Chinese Academy of Science, SIAT, Shenzhen, China

[3] School of Environment and Spatial Informatics, China University of Mining & Technology, Xuzhou 221116, China

criterion, MRF takes full advantage of the spectral characteristic of pixels and the label field characteristic of their neighborhoods, and finally provides the optimal image analysis results by solving the minimum of the sum of characteristic energy of the two [18, 20, 24]. However, in an MRF, because of the inaccuracy in defining the spatial relationship among the pixels in the neighborhood and setting the weights of spatial information, the spatial information cannot be fully and reasonably utilized [2, 14, 15]. Hence, an over-smooth change map will be finally brought without accurate spatial relationships between neighborhoods and weights for the spatial information [3, 17].

In order to solve these problems, this paper proposed an improved MRF method to change detection by focusing on the determination of the weights of spatial information and the definition of the spatial relationship between neighborhood pixels. Firstly, the difference image is obtained using change vector analysis (CVA) method. Secondly, the fuzzy c-means (FCM) clustering algorithm is implemented to the difference image, in which membership degree and centers of changed and unchanged parts are obtained. The linear spatial weights are then computed through diving the difference image into unchanged, uncertainty and changed regions based on the gray values of pixels. Additionally, the spatial attraction model is also introduced to refine spatial relationships between neighborhood pixels to improve the accuracy of spatial information. Finally, the improved MRF is applied to detect changes. To evaluate the effectiveness of proposed method, two experiments were carried on satellite images. The paper is organized as follows. Section 2 shows the related works, and the improved MRF method for change detection is proposed in the Section 3, Section 4 designed some experiments to verify the proposed method. Finally, Section 5 draws conclusions.

2 Related works

In the past three decades, so many change detection methods have been devolved, which can be grouped into three stages. In the first stage, changes are found by comparing the multitemporal images using simple algebra methods, such as image differencing, image ratio, image regression and CVA, etc. [13, 21]. However, simple algebra methods need a threshold to identify changes, and it was usually decided manually. Therefore, many automatic methods for finding the optimal threshold were proposed in the second stage [16]. Nevertheless, a new problem was found that only spectral information is exploited resulting in much noise contained in the change map. In the third stage, more methods were implemented to the difference image generated by image differencing or CVA combing spectral and spatial information, and MRF is one of the most effective methods [2]. But it results in an over-smooth change map that the spatial information cannot be fully and reasonably utilized in the MRF. The edge information was integrated into the spatial energy function of MRF to preserve small structures and edges [3, 12]. But there are still have some shortcomings, on the one hand paper does not provide good results for objects with occlusion/disocclusion the other hand if the object of interest has cast shadows in the scene, the proposed scheme does not yield good results. The method proposed in paper [16] obtains accurate and robust classification maps for different kinds of images.

In order to solve the above problems, lots of researchers did a lot work and gain some results. The spatial attraction was introduced into the spatial energy function to replace the equivalent value in the Kronecker delta function of MRF [5, 23], which reduced over-smooth results. Additionally, a custom-designed Potts model was proposed to improve the accuracy of weights for the spatial information [6]. But the effects of weight for the spatial information and

spatial relationships between neighborhood pixels haven't been considered together. Therefore, this paper proposes an improved MRF by enhancing the accuracy of spatial information to improve the accuracy of change-detection results.

3 Proposed method

To solve the aforementioned problem, a change-detection method based on the improved MRF is proposed. Figure 1 shows the detailed flow chart of proposed method, and the specific procedures are presented as follows.

3.1 Fuzzy clustering for the difference image

(1) The differential image is obtained by processing the remote-sensing images at two time phases through change vector analysis.

Suppose the images at t_1 and t_2 are denoted as $X_1=\{x_1^b(i,j)|1\le i\le m,1\le j\le n,1\le b\le L\}$ and $X_2=\{x_2^b(i,j)|1\le i\le m,1\le j\le n,1\le b\le L\}$, respectively, in which m, n, and L are the numbers of rows, columns, and bands of the image; $x_1^b(i,j)$ and $x_2^b(i,j)$ denote the gray values of the pixels at row i, column j in the b-th band at two time phases, respectively. The change vector can be calculated by the following equation [11]:

$$\Delta X = X_1 - X_2 = \begin{pmatrix} x_1^1(i,j)-x_2^1(i,j) \\ x_1^2(i,j)-x_2^2(i,j) \\ \cdots \\ x_1^L(i,j)-x_2^L(i,j) \end{pmatrix}. \tag{1}$$

The change intensity of the pixel can be expressed by the following Euclidean distance:

$$\|\Delta X\| = \sqrt{\sum_{b=1}^{L}\left(x_1^b(i,j)-x_2^b(i,j)\right)^2}. \tag{2}$$

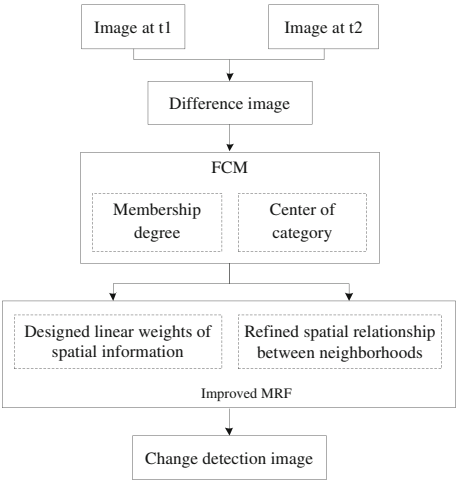

Fig. 1 Flow chart of the proposed method

ΔX includes the information on category change of surface features in two images at two time phases, and $\|\Delta X\|$ denotes the difference of gray level of two images at two time phases. According to Eq. (2), the differential image $X=\|\Delta X\|=\{x(i,j)|1\le i\le m, 1\le j\le n\}$ can be obtained.

(2) The differential images are clustered using the FCM algorithm and classified into unchanged and changed categories. The membership degree u_{ij} of the pixel x_j to the i-th category, and the centers of these two categories, C_1 and C_2, are calculated.

Fuzzy clustering was first proposed by Dunn [8] and improved into a classical FCM clustering algorithm by Bezdek [9]. Suppose $X=\{x_1,x_2,\cdots,x_N\}$ is a dataset consisting of N vectors and fuzzily divided into C categories. $u_{ik}(1\le k\le c)$ denotes the degree of membership of the datum x_i in the dataset X to the k-th category. The fuzzy division results can be described using the matrix $U=\{u_{ik}\}$, which meets the following constraint conditions:

$$\begin{aligned} &u_{ik}\in[0,1],\forall i,k\\ &\sum_{k=1}^{c} u_{ik}=1,\forall i\\ &0<\sum_{i=1}^{N} u_{ik}<N,\forall k \end{aligned} \quad . \tag{3}$$

The FCM clustering algorithm conforms to the principle that the sum-of-squared differences between each sample and the mean value of the located category are minimum. The objective function Jreaches the minimum by iterating and updating the membership matrix U and the clustering center V. Thus, optimal clustering can be achieved. The objective function is expressed as

$$J(U,V)=\sum_{i=1}^{N}\sum_{k=1}^{c}(u_{ik})^q\|x_i-v_k\|^2 \tag{4}$$

where $U=\{u_{ik}\}$ is the membership matrix that satisfies Eq. (3), $V=\{v_1,v_2,\cdots,v_c\}$ denotes the set of clustering centers, and $q\in[1,+\infty)$ denotes the weighted index, which is used to control the fuzzy degree of clustering results. When $q=1$, the fuzzy clustering belongs to traditional c-means clustering. In general, when $q=2$, the calculation is simple and the results are ideal. When fuzzy clustering is performed on differential images, the sample x_i can be replaced by x_{ij} to represent the gray value of the pixel at (i,j) and v_k denotes the mean of the k-th category. Thus, Eq. (4) can be expressed as

$$J(U,V)=\sum_{\substack{1\le i\le m\\ 1\le j\le n}}\sum_{k=1}^{c}(u_k(i,j))^2\|x(i,j)-v_k\|^2 \tag{5}$$

where $u_k(i,j)$ denotes the degree of membership of the pixel (i,j) to the k-th class and $\|\cdot\|$ denotes the Euclidean distance. The specific procedure of FCM clustering algorithm is presented as follows:

1) The number of categories in clustering is set as N, and the clustering center $V=\{v_1,v_2,\cdots,v_c\}$ is initialized.
2) The matrix of fuzzy membership is calculated according to the following equation:

$$u_k(i,j)=\left[\sum_{p=1}^{c}\left[\frac{\|x(i,j)-v_k\|}{\|x(i,j)-vp\|}\right]^2\right]^{-1}. \tag{6}$$

3) The clustering center is updated based on the following equation:

$$v_k=\frac{\sum_{\substack{1\le i\le m\\1\le j\le n}} u_k(i,j)^2 x(i,j)}{\sum_{\substack{1\le i\le m\\1\le j\le n}} u_k(i,j)^2}. \tag{7}$$

4) The convergence of Eq. (5) is judged as follows. When $\|V^{t+1}-V^t\|<\varepsilon$ (t is the number of iterations and $\varepsilon>0$ indicates the stopping of computation), Eq. (5) is convergent and the iteration stops; otherwise, steps 2 and 3 are repeated until Eq. (5) is convergent.

Finally, after processing by FCM clustering, the membership degrees of each pixel and the central values of each category can be obtained.

3.2 Markov random field model

Using MAP criterion, MRF is an image processing method that combines spectral and spatial information. From the perspective of field energy, the sum of energy of spectral characteristic field and label field of each pixel should be minimized so that the optimal result can be obtained [10].

Suppose $X=\{x_1,x_2,\cdots x_n\}\subset R^d$ denotes the remote-sensing dataset composed of n vectors in d-dimensional Euclidean space (n is the number of pixels and d is the number of bands), $L=\{l_1,l_2,\cdots l_c\}$ denotes the category label for each pixel and c is the number of categories. Generally, the ultimate category of images can be determined using the MAP criterion, and the formula is

$$L=\arg\max\{P(L)p(X|L)\}, \tag{8}$$

where $P(L)$ denotes the prior probability of a category label in the dataset, and $p(X|L)$ denotes the conditional probability density function of the pixel in the dataset. Based on the MRF model, the maximum posterior probability can be obtained by solving the minimum of energy function $U_{MRF}(x_i)$ as follows:

$$U_{MRF}(x_i)=U_{spectral}(x_i)+U_{spatial}(x_i), \tag{9}$$

where $U_{spectral}(x_i)$ denotes the energy function of spectral characteristic field of pixel x_i, and $U_{spatial}(x_i)$ denotes the spatial energy function of the pixel x_i in local neighborhood.

The energy function of spectral characteristic field of pixel x_i can be expressed as

$$U_{spectral}(x_i)=\frac{1}{2}\ln\left|2\pi\sigma_k^2\right|+\frac{1}{2}(x_i-\mu_k)^2\left(\sigma_k^2\right)^{-1}, \tag{10}$$

where μ_k and σ_k^2 denote the mean and variance of pixel gray values in the$k$-th category, respectively. These two values can be calculated by the initial change-detection images generated in FCM clustering.

The spatial label field energy of the pixel x_i can be calculated by

$$U_{spatial}(x_i) = \beta \sum_{j \in N_i} I\left(l(x_i), l\left(x_j\right)\right), \tag{11}$$

$$I\left(l(x_i), l\left(x_j\right)\right) = \begin{cases} -1 & l(x_i) = l\left(x_j\right) \\ 0 & l(x_i) \neq l\left(x_j\right) \end{cases}, \tag{12}$$

where $\beta>0$ denotes the penalty coefficient defined by the same user, which is used to control the effect of the neighboring pixel of pixel x_i on x_i; N_i denotes the spatial neighborhood ($i \notin N_i$) of the pixel x_i; $l(x_i)$ and $l(x_j)$ ($(j \in N_i)$) denote the category labels of the pixel x_i and its neighboring pixel x_j, respectively. As described in MRF theory, the spatial relation between pixels in the label field can be expressed by the neighborhood system N_i and defined by the Potts model in Eq. (12).

Change detection is a discrete combinational optimization problem, and the analysis results can be acquired only by the global or local optimization based on the iterative search method [20]. In this paper, iterated conditional mode (ICM) was used to search for the optimal result of Eq. (9) to solve the minimum value of energy function and analyze the remote-sensing images. ICM refers to the process where the local energy is calculated using local conditional probability, and then the analysis results of images with minimum local energy are obtained by updating the labels of images point by point.

3.3 Designed linear spatial weights of MRF

In the MRF, when the label field energy is calculated using the Potts model, the adopted weights β are the same for all the pixels in differential images without any consideration of the distribution of pixel gray values in differential images. In a differential image, the pixels have different gray values and therefore different probability to change. For a pixel, the larger the gray value is, the greater the probability of change is; on the contrary, the smaller the gray value is, the greater is the probability to remain unchanged. For the pixels with intermediate gray level, determining whether the change exists based solely on gray value is difficult. In the traditional Potts model, all the pixels in differential images are set with the same penalty coefficient β. For the pixels with extremely large or extremely small gray values, this setting easily causes an overuse of spatial neighborhood information, which leads to the oversmoothing on the changed regions.

Based on the centers of the two categories calculated using the FCM algorithm, two threshold values, T_1 and T_2, are set. The differential image is then divided into three parts (changed, uncertain, and unchanged), and the corresponding penalty coefficients are calculated. Thus, the contrast-sensitive Potts model is established.

In the traditional MRF, the energy of the spatial label field of the pixel x_i can be calculated by [6, 22, 25]

$$U_{spatial}(x_i) = \sum_{j \in N_i} I\left(l(x_i), l\left(x_j\right)\right), \tag{13}$$

$$I\left(l(x_i), l\left(x_j\right)\right) = \beta \begin{cases} -1 & l(x_i) = l\left(x_j\right) \\ 0 & l(x_i) \neq l\left(x_j\right) \end{cases}, \tag{14}$$

where $\beta>0$ denotes the penalty coefficient defined by the user and is employed to control the effect on the pixel x_i from its neighboring pixel; N_i denotes the spatial neighborhood ($i \notin N_i$) of the pixel x_i; $l(x_i)$ and $l(x_j)(j \in N_i)$ denote the category labels of pixel x_i and the neighboring pixel x_j, respectively.

According to the centers of the two categories, C_1 and C_2, the threshold values T_1 and T_2 were set. As shown in Fig. 2, the pixels in the differential image can be divided into three parts, namely, changed, uncertain, and unchanged. The threshold values T_1 and T_2 can be calculated by

$$\begin{cases} T_1 = M_{mid} - \alpha_1 (M_{mid} - C_1) \\ T_2 = M_{mid} + \alpha_2 (C_2 - M_{mid}) \end{cases}, \tag{15}$$

where M_{mid} denotes the central pixel and has the same membership degree as the changed and unchanged categories when FCM is used; and both α_1 and α_2 are constants that are used to adjust the range of the three parts.

On this basis, three strategies are proposed to calculate the adaptive penalty coefficient β_m in the Potts model for the three parts.

$$\beta_m(X(i,j)) = \begin{cases} \beta \dfrac{X(i,j) - X_{\min}}{T_1 - X_{\min}} & X(i,j) < T_1 \\ \beta & T_1 \le X(i,j) \le T_2 \\ \beta \dfrac{X_{\max} - X(i,j)}{X_{\max} - T_2} & X(i,j) > T_2 \end{cases}, \tag{16}$$

where $X_{\min}$ and $X_{\max}$ denote the maximum and minimum gray values in the differential image, respectively. By replacing the traditional penalty coefficient β with the adaptive penalty coefficient β_m, we can construct a contrast-sensitive Potts model.

Under this condition, when the gray value of the pixel is less than the threshold value T_1, the penalty coefficient β_m decreases linearly as the gray value varies from T_1 to $X_{\min}$. Accordingly, the effects of spatial neighborhood information on the pixels with relatively small gray values can be reduced because these pixels are highly likely to remain unchanged. When the gray value of the pixel is larger than T_2, the penalty coefficient β_m decreases linearly as the gray value increases from T_2 to $X_{\max}$. In this way, the effects of spatial neighborhood information on the pixels with relatively large gray values can be reduced because these pixels are highly likely to change. Additionally, for the pixels in the uncertain part, we set a constant

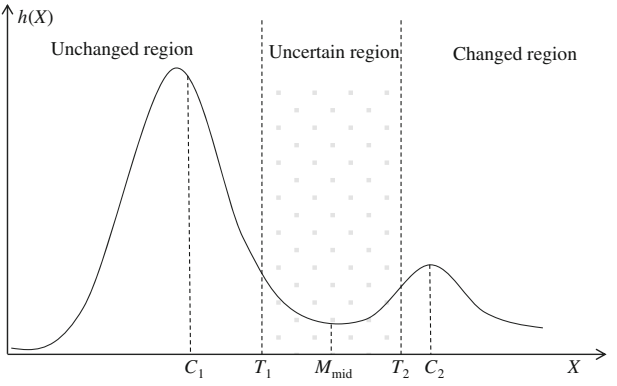

Fig. 2 Changed, uncertain, and unchanged parts in differential image

penalty coefficient β. Thus, the initial change-detection image can be refined by taking full advantage of spatial information.

3.4 Refined spatial relationship between neighborhoods of MRF

Figure 3 presents the label field of spatial neighborhood when the conventional MRF is used for change detection, where i,j denotes the pixel in row i, column j; 0 indicates no change in the pixel; and 1 indicates change in the pixel. The spatial neighborhood relation between various pixels can be characterized by comparing the numbers of pixels of different categories in the neighborhood. Many mixed pixels are included because of the complexity of surface features and the limitations in the spatial resolution of remote-sensing images. Therefore, the spatial neighborhood relation between pixels cannot be accurately expressed by arbitrarily labeling the neighboring pixels as 0 and 1.

The spatial gravity model is used to introduce the membership information to an MRF so that the spatial relationship between neighboring pixels can be identified accurately.

The surface features and the interaction between surface feature and sensor are highly complex, and the spatial resolution of the sensor is limited. Therefore, numerous mixed pixels are included in images. In the traditional Potts model, the spatial neighborhood relation between pixels is usually defined as 0 or 1, which is too absolute and not accurate. This method easily causes the overuse of spatial information and oversmoothing of the change-detection results. The Potts model can be modified by introducing the spatial gravity model to the degree of membership. The spatial neighborhood relation between pixels can be redefined, and Eq. (12) can be rewritten as

$$I\left(l(x_i), l\left(x_j\right)\right) = \begin{cases} -w_{ij} & l(x_i) = l\left(x_j\right) \\ 0 & l(x_i) \neq l\left(x_j\right) \end{cases}, \tag{17}$$

where w_{ij} denotes the spatial gravity between the pixel x_i and the neighboring pixel x_j, and can be calculated by the following equation [5, 23]:

$$w_{ij} = z(p_i) \times z(p_i) \times \frac{1}{R_{i,j}^2}, \tag{18}$$

1	1	0
1	i, j	0
0	0	0

Fig. 3 Label field of spatial neighborhood in MRF

where i is the index value of the central pixel x_i; $j \in N_i\{j=1,2,\cdots,8\}$ denotes the pixels in the neighborhood of central pixel x_i in a 3*3 pixel window, as shown in Fig. 4a; z denotes the category label of the central pixel x_i; p_i and p_j denote the membership degrees of the pixel x_i and the neighboring pixel x_j with regard to the class z, and can be calculated using the FCM clustering algorithm; R_{ij} denotes the spatial distance between the central pixel x_i and the neighboring pixel x_j, as shown in Fig. 4b.

4 Results and analysis

To verify the feasibility of the proposed method, we selected two groups of remote-sensing images for change detection. Comparisons were made between the proposed method, the multiresolution level set (MLS), MLS with Kittler algorithm (MLSK) [1], FCM, the combination of expectation maximization (EM) and MRF [13], and the combination of FCM and MRF. Three indices are used to evaluate the results: 1) missed detection (*MD*): the number of changed pixels incorrectly classified as unchanged. The missed detection rate P_m is calculated by the ratio $P_m = MD/N_0 \times 100\%$, here N_0 is the total number of changed pixels counted in the ground reference map; 2) false alarm (*FA*): the number of unchanged pixels wrongly detected as changed. The false detection rate P_f is described by the ratio $P_f = FA/N_1 \times 100\%$, where N_1 is the total number of unchanged pixels counted in the ground reference map; 3) total error (*TE*): the total number of detection error including both miss and false detection, which is the sum of the *MD* and the *FA*. Hence, the total error rate P_t is described using $P_t = (FA+MD)/(N_0+N_1) \times 100\%$ [7, 19].

4.1 Experiment of Landsat 7 ETM+ data set

In Experiment 1, we used two remote-sensing images of a certain region in Liaoning province collected by Landsat 7 ETM+ satellite sensor in August 2001 and August 2002.

The images with the size of 300×280 pixels were selected as the study area, as shown in Fig. 5a and b, corresponding to the true-color remote-sensing images at two time phases. The image at t_1 was registered to the image at t_2, and the relative radiometric normalization was

$N_{i,1}$	$N_{i,2}$	$N_{i,3}$
$N_{i,4}$	i	$N_{i,5}$
$N_{i,6}$	$N_{i,7}$	$N_{i,8}$

(a) Neighborhood x_i of central pixel N_i

$1/\sqrt{2}$	1	$1/\sqrt{2}$
1	i	1
$1/\sqrt{2}$	1	$1/\sqrt{2}$

(b) Distance between central pixel x_i and its neighborhood N_i

Fig. 4 Spatial neighborhood of central pixel x_i

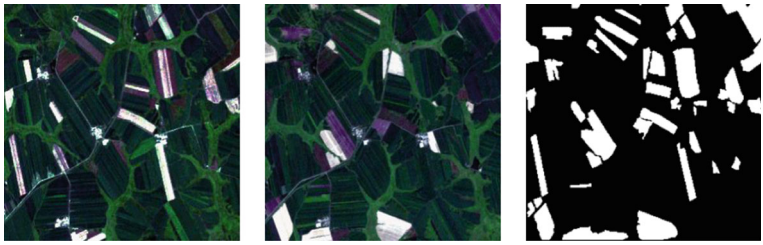

(a) Image at time phase t_1 (b) Image at time phase t_2 (c) Ground reference data

Fig. 5 Landsat 7 ETM+ data adopted in Experiment 1

conducted on them by histogram matching. Subsequently, change vector analysis was used to process the images within all bands except thermal infrared band, and the differential images were acquired. The ground reference data were artificially generated by comparing the images at two time phases, as shown in Fig. 5c.

Figure 6 shows the change-detection images obtained by MLS, MLSK, FCM, EM, MRF. In the detections with multiscale-level set method (MLS) and threshold-based MLS (MLSK), μ=0.2, which referenced the initial paper [1]. As shown in Fig. 6a and b, the obtained change-detection images using MLS and MLSK are highly similar to the ground reference data; however, speckle noise can be observed in some comparatively large regions of change, e.g., Region A in the figure.

When MRF and the proposed method are used, the values of β are set to be 1.8 and 1, respectively, where the parameter was first set as an empirical value 1.6 and then found the

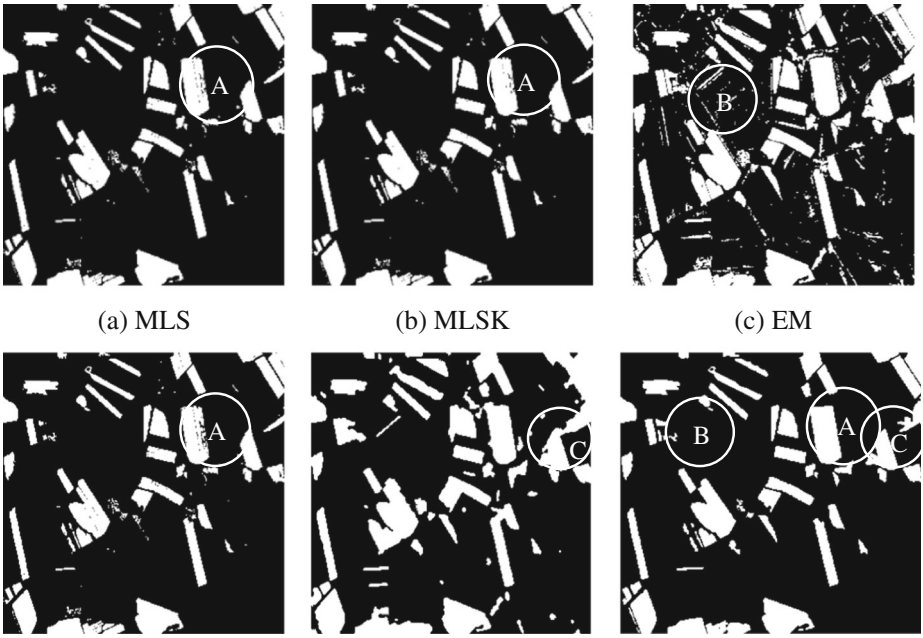

(a) MLS (b) MLSK (c) EM

(d) FCM (e) MRF (f) Proposed method

Fig. 6 Change-detection results of data in Experiment 1

optimal value manually. As shown in Region B in Fig. 6c and Region A in Fig. 6d, a great deal of speckle noise exists in the change-detection images when expectation maximization (EM) and FCM algorithms are used because the spatial neighborhood information is not considered, where the weighting exponent of FCM was set to 2. Although the change-detection regions in Fig. 6e and f are more complete than those in the other four images, more details are retained when the proposed method are used, which also eliminates the oversmoothing phenomena of borders in traditional MRF, as shown by Region C in the figures. In conclusion, the change-detection image generated by the proposed method is most similar to the ground reference data.

Table 1 presents the comparisons of the falsely detected pixels, undetected pixels, and total errors for MLS, MLSK, EM, FCM, MRF, and the proposed method. One can conclude that, compared with the other five methods, the total error rate of the proposed method was reduced by 1.2, 1.2, 4.2, 1.4, and 2.5 %, respectively. At least 1000 errors were reduced, and the change-detection results using the proposed method have the highest accuracy. However, since the proposed the proposed method combines FCM and MRF, the calculation time is longer than that for the single FCM and MRF.

4.2 Experiment of Landsat 5 TM data set

In Experiment 2, we used the images of a certain region in Alaska, USA collected by the Landsat 5 TM sensor in July 1985 and July 2005.

The images with a size of 400×400 pixels were selected in the present study, as shown in Fig. 7a and b, corresponding to the true-color remote-sensing images at two time phases. The image at t_1 was registered to the image at t_2, and the relative radiometric normalization was conducted on the images by histogram matching. The ground reference data were artificially generated by comparing the images at two time phases, as shown in Fig. 7c.

Figure 8 shows the obtained change-detection results using MLS, MLSK, EM, FCM, MRF, and the proposed method. When MLS and MLSK were used, the parameter μ was set as 0.2. When MRF and the proposed method were used, the parameter β was set as 1.5 and 0.8, respectively.

As shown in Fig. 8a and b, numerous change details are lost in the results by MLS and MLSK (see Region A). As shown in Fig. 8c, a significant amount of speckle noise is included (see Region B), mainly because the EM algorithm detects the changes only by setting the threshold and not by utilizing spatial information. Since a large number of

Table 1 Accuracy of change detection in Experiment 1

Method	Falsely detected errors		Undetected errors		Total errors	
	Number of pixels	P_f (%)	Number of pixels	P_m (%)	Number of pixels	P_t (%)
MLS	722	1.1	3086	18.7	3808	4.5
MLSK	721	1.1	3054	18.6	3775	4.5
EM	5420	5.3	863	8.1	6283	7.5
FCM	669	1.0	3294	20.0	3963	4.7
MRF	4202	6.2	725	4.4	4927	5.8
Proposed method	746	1.1	1987	12.1	2733	3.3

(a) Image at time phase t_1 (b) Image at time phase t_2 (c) Ground reference data

Fig. 7 Landsat 5 TM data adopted in Experiment 2

mixed pixels existed and the categories of pixels were labeled as those with a greater degree of membership when FCM was used, many change details were undetected, e.g., the results in Region A in Fig. 8d. The proposed method not only generates a more complete homogeneous region but also detects many change details. Comparatively, the single MRF method makes the change-detection results oversmoothed, as shown in Region C in Fig. 8e and f. Conclusively, compared with the change-detection image generated by the other methods, the image generated by the proposed method is closest to the ground reference data.

Table 2 lists the accuracy of change-detection results by MLS, MLSK, EM, FCM, MRF, and the proposed method, respectively. Since the membership information calculated by FCM

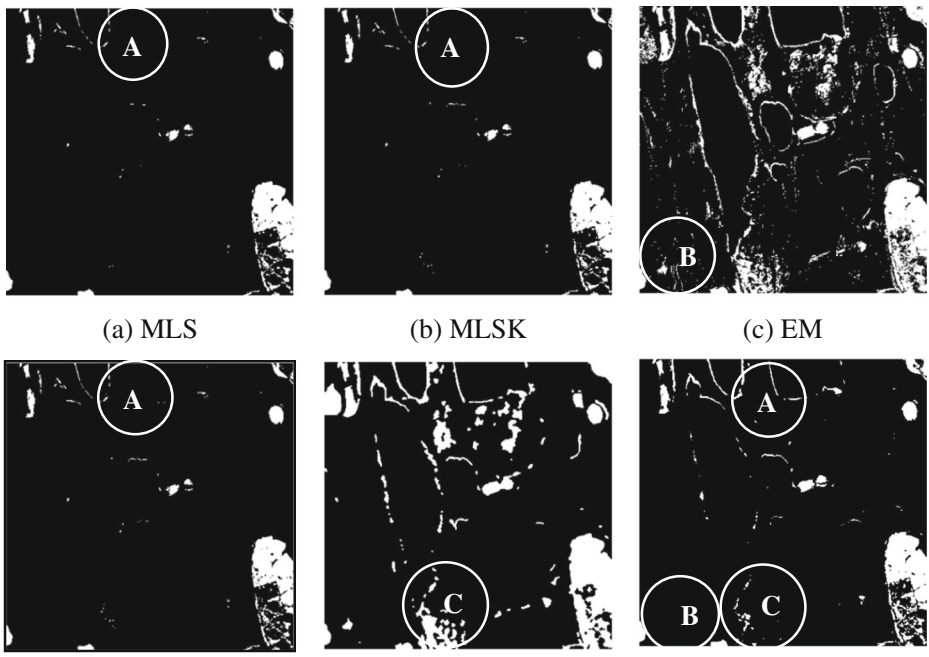

(a) MLS (b) MLSK (c) EM

(d) FCM (e) MRF (f) Proposed method

Fig. 8 Change-detection results of data in Experiment 2

Table 2 Accuracy of change detection in Experiment 2

Method	Falsely detected errors		Undetected errors		Total errors	
	Number of pixels	P_f (%)	Number of pixels	P_m (%)	Number of pixels	P_t (%)
MLS	128	0.1	3639	37.4	3767	2.4
MLSK	138	0.1	3597	36.9	3735	2.3
EM	9323	6.2	107	1.1	9430	5.9
FCM	118	0.1	3595	36.9	3713	2.3
MRF	9042	6.0	449	4.6	9491	5.9
Proposed method	503	0.3	1542	15.8	2045	1.3

was introduced to an MRF through the spatial gravity model, the spatial neighborhood relation between pixels can be defined more accurately. The proposed method compared with other methods, its total error rate was reduced by 1.1, 1.0, 4.6, 1.0 and 4.6 %, respectively, reduced at least more than 1500 errors of pixels, can generate the highest accuracy of change detection results. These results verify that the proposed method is feasible.

5 Conclusion

By improving the weights for spatial information and spatial relationships between neighborhood pixels of MRF, an improved MRF is proposed to change detection. The results of the two experiments indicate that, compared with MLS, MLSK, and FCM, the changed region detected by the proposed method is more complete. Compared with EM and MRF, the proposed method can be used to remove the speckle noise effectively. Besides, it can avoid the oversmoothing of the changed region obtained by MRF to a certain degree. Overall, compared with MLS, MLSK, EM, FCM, and MRF, the proposed method can generate a change-detection image closer to the ground reference data, achieving higher accuracy of change detection. The experimental results suggest that the designed linear weights for the spatial information and redefined the spatial neighborhood relation between pixels in the label field of MRF are feasible, which can provide more accurate results than those using the Potts model in traditional MRF. Therefore, the proposed method is a more accuracy approach to change detection for remotely sensed images. However, the proposed method generates more accurate results by combing FCM and MRF, it needs more computing time. Hence, when we want to obtain more accurate results, it is better to adopt the proposed one, whereas, when the change maps need producing in shorter time, other methods used in this paper should be exploited. In the future, an adaptive widow of MRF is worth studying to improve its robustness for different kinds of noise.

Acknowledgments Research reported in this paper was supported by the Natural Science Foundation of China (No. 51304199); the Open Projects of "State Key Laboratory of Coal Resources and Safe Mining, CUMT" (No.SKLCRSM13X08);the Fundamental Research Funds for the Central Universities (NO. 2014XT01).

Conflict of interests The authors declare that there is no conflict of interests regarding the publication of this article.

References

1. Bazi Y, Melgani F, Al-Sharari HD (2010) Unsupervised change detection in multispectral remotely sensed imagery with level set methods. IEEE Trans Geosci Remote Sens 48(8):3178–3187
2. Chen Y, Cao Z (2013) An improved MRF-based change detection approach for multitemporal remote sensing imagery. Signal Process 93(1):163–175
3. Ghosh A, Subudhi BN, Ghosh S (2012) Object detection from videos captured by moving camera by fuzzy edge incorporated Markov random field and local histogram matching. IEEE Trans Circuits Syst Video Technol 22(8):1127–1135
4. Gong MG, Su LZ, Jia M, Chen WS (2014) Fuzzy clustering with a modified MRF energy function for change detection in synthetic aperture radar images. IEEE Trans Fuzzy Syst 22(1):98–109
5. Hao M, Zhang H, Shi WZ, Deng KZ (2013) Unsupervised change detection using fuzzy c-means and MRF from remotely sensed images. Remote Sens Lett 4(12):1185–1194
6. Hao M, Shi W, Deng K, Zhang H (2014) A contrast-sensitive Potts model custom-designed for change detection. Eur J Remote Sens 47:643–654
7. Hao M, Shi W, Deng K, Zhang H (2015) Fusion-based approach to change detection to reduce the effect of the trade-off parameter in the active contour model. Remote Sens Lett 6(1):39–48
8. Jiachen Y et al (2015) Objective evaluation criteria for stereo camera shooting quality under different shooting parameters and shooting distances. IEEE Sensors J 15(8):4508–4521
9. Jiang D, Xu Z, Zhang P, Zhu T (2014) A transform domain-based anomaly detection approach to network-wide traffic. J Netw Comput Appl 40:292–306
10. Li X, Lv Z, Hu J, Yin L, Zhang B, Feng S (2015) WebVRGIS based traffic analysis and visualization system. Adv Eng Softw: In press
11. Liu S, Fu W, Zhao W (2013) A novel fusion method by static and moving facial capture [J]. Math Probl Eng 2013:1–6
12. Liu S, Cheng X, Fu W et al (2014) Numeric characteristics of generalized M-set with its asymptote [J]. Appl Math Comput 243(9):767–774
13. Liu S, Fu W, He L, et al (2015) Distribution of primary additional errors in fractal encoding method [J]. Multimedia Tools Appl: In press
14. Liu S, Zhang Z, Qi L, et al (2015) A fractal image encoding method based on statistical loss used in agricultural image compression [J]. Multimedia Tools Appl: In press
15. Lv Z, Tek A, Da Silva F, Empereur-Mot C, Chavent M, Baaden M (2013) Game on, science-how video game technology may help biologists tackle visualization challenges [J]. PLoS One 8(3):e57990
16. Lv Z, Halawani A, Feng S, Li H, Ur Réhman S (2014) Multimodal hand and foot gesture interaction for handheld devices [J]. ACM Trans Multimed Comput Commun Appl 11(1s):10:1–10:19
17. Lv Z, Halawani A, Feng S, ur Rehman S, Li H (2015) Touch-less interactive augmented reality game on vision based wearable device [J]. Pers Ubiquit Comput 19(3–4):551–567
18. Melgani F, Bazi Y (2006) Markovian fusion approach to robust unsupervised change detection in remotely sensed imagery. IEEE Geosci Remote Sens Lett 3(4):457–461
19. Shi W, Hao M (2013) Analysis of spatial distribution pattern of change-detection error caused by misregistration. Int J Remote Sens 34(19):6883–6897
20. Xiong BL, Chen Q, Jiang YM, Kuang GY (2012) A threshold selection method using Two SAR change detection measures based on the Markov random field model. IEEE Geosci Remote Sens Lett 9(2):287–291
21. Yetgin Z (2012) Unsupervised change detection of satellite images using local gradual descent. IEEE Trans Geosci Remote Sens 50(5):1919–1929
22. Zhang H, Shi W, Liu K (2012) Fuzzy-topology-integrated support vector machine for remotely sensed image classification. IEEE Trans Geosci Remote Sens 50(3):850–862
23. Zhang H, Shi W, Wang Y, Hao M, Miao Z (2014) Spatial-attraction-based Markov random field approach for classification of high spatial resolution multispectral imagery. IEEE Geosci Remote Sens Lett 11(2):489–493
24. Zheng ZG, Jeong HY, Huang T et al (2015) KDE based outlier detection on distributed data streams in sensor network [J]. J Sens 2015:1–11
25. Zheng ZG, Wang P, Liu J et al (2015) Real-time Big data processing framework: challenges and solutions [J]. Appl Math Inf Sci 9(6):2217–2237

Wei Gu is an Associate Professor at the State Key Laboratory of Coal Resources and Mine Safety, School of Mines, China University of Mining & Technology. He received his Doctoral degree China University of Mining and Technology in 2013, China. His researches interests include image processing, information extraction from remote sensing images and remote sensing image fusion.

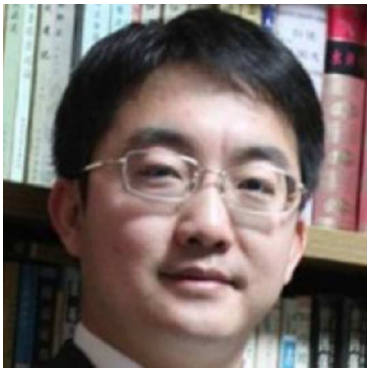

Zhihan Lv is an engineer and researcher of virtual/augmented reality and multimedia major in mathematics and computer science, having plenty of work experience on virtual reality and augmented reality projects, engage in application of computer visualization and computer vision. His research application fields widely range from everyday life to traditional research fields (i.e., geography, biology, medicine). During the past years, he has finished several projects successfully on PC, Website, Smartphone and Smartglasses. In 2012, he was granted PhD. degree in Computer applied technology from Ocean university of China (2006–2012). Before that, he has enjoyed 16 months full-time research experience at Centre national de la recherchescientifique(CNRS)-UPR9080 in Paris (2010–2011). After then, he has fulfilled 2-year postdoc research experience at Umea University and a short invited teaching experience at KTH Royal Institute of Technology in Sweden. Since 2012, he has held an adjunct assistant professor position at Chinese Academy of Science.

Ming Hao is a postdoctoral researcher at theSchool of Environmental Science and Spatial Informatics, China University of Mining and Technology. He received his Doctoral degree in China University of Mining and Technology in 2015, China. His research interests include image processing, information extraction from remote sensing images and remote sensing image fusion.